IL NUOVO CIMENTO Vol. 36 C, N. 4 Luglio-Agosto 2013
DOI 10.1393/ncc/i2013-11551-1

Communications: SIF Congress 2012

ESR spectroscopy for analyzing the spatial distribution of free radicals in ammonium tartrate

M. Marrale(*)

Dipartimento di Fisica e Chimica, Università di Palermo
Viale delle Scienze Edificio 18, 90128 Palermo, Italy

ricevuto il 15 Gennaio 2013

Summary. —
In the last few years the worldwide spread of radiation therapy with hadrons has stimulated the research on the effects produced by these particles on biological systems. This investigation on complex systems (such as cells) is aided by the study of the effects on simpler organic compounds in order to better model how the defects are produced by various types of ionizing radiations. Among the various experimental techniques the contribution of electron spin resonance (ESR) spectroscopy is valuable because it does measure not only the total number of radiation-induced defects (and therefore the absorbed dose), but it can also provide useful information on the distribution of defects inside the matter and therefore on the linear energy transfer (LET) and quality of the radiations. In this work the applications of three experimental ESR methods for discriminating radiations with different quality on ammonium tartrate samples are reviewed. In particular, continuous wave ESR (cw-ESR) spectroscopy allows to measure the ESR signal saturation with microwave power, whereas pulsed ESR spectroscopy permits to measure the microscopic local concentration by means of the analysis of the instantaneous diffusion and to measure the distance distribution through the Double Electron-Electron Resonance (DEER).

PACS 87.64.-t – Spectroscopic and microscopic techniques in biophysics and medical physics.
PACS 76.30.-v – Electron paramagnetic resonance and relaxation.
PACS 76.30.Rn – Free radicals.
PACS 87.53.Bn – Dosimetry/exposure assessment.

1. – Introduction

The continuously increasing worldwide spread of applications of ionizing radiations for cancer therapy has led the research towards a deeper understanding of the interactions of these particles with biological systems. Nowadays, the hadron therapy with protons

(*) E-mail: maurizio.marrale@unipa.it

or other ions (such as carbon ions) arouses large interest among the radiation oncologists because of the larger effectiveness of these charged particles in killing tumoral cells with respect to conventional radiation beams (such as photons and electrons). The knowledge of the details of the energy release of these particles inside the matter as well as the modeling of the biological damage induced by various ionizing radiations become fundamental for the development of this promising cancer treatment activity ([1] and references therein). The inverse depth dose profile (which brings about a larger dose release in depth than in entrance) of ions makes these particle suitable for hitting deep tumors significantly reducing the dose on the healthy tissues. In the last decades there is also a growing interest towards the Boron Neutron Capture Therapy (BNCT) performed by concentrating ^{10}B nuclei inside the tumor cells which subsequently are irradiated with thermal neutrons. The reaction of thermal neutrons with the ^{10}B nuclei gives rise to α-particles and ^{7}Li ions releasing energy inside the tumor cells and provoking the death of these malignant cells [2].

In order to increase the effectiveness of these novel radiation therapies new dosimetric methods able to investigate the microscopic and nanoscopic distribution of the defects produced by ionizing radiations in passing through the matter have been developed. These microdosimetric and nanodosimetric techniques can provide information also on the linear energy transfer (LET) of the radiation and therefore are able to distinguish radiations with different quality. Since the biological effects depend on the radiation quality and on the LET of the radiations, microdosimetry and nanodosimetry are essential for furnishing valuable information from a radiobiological point of view. Among the various microdosimetric techniques the tissue equivalent proportional counters, the chemically etched track detectors [3], the gel dosimeters [4], the thermoluminescent dosimeters through the high-temperature ratio method [5], and solid-state microdosimeters [6] can be counted.

In this paper the contribution of the electron spin resonance (ESR) to the analysis of the radiation-induced defects and their spatial distribution in ammonium tartrate pellets is reviewed. In particular, the ESR can quantify the energy released per unit mass (*i.e.* absorbed dose) by measuring the concentration of free radicals produced by ionizing radiations. In the last three decades the ESR spectroscopy is providing an important contribution to dosimetry in both industrial field, radiation therapy and retrospective reconstruction of dose [7]. Indeed, nowadays ESR dosimetry is recognized as standard dosimetric technique for three applications: alanine/ESR dosimetry, the procedures for identification of irradiated foodstuffs containing cellulose and bone material [7].

The ESR is also a powerful tool for getting information on the distribution of radiation-induced free radicals inside matter. This is because the ESR signal depends on the longitudinal and transversal relaxation times (T_1 and T_2, respectively) and these relaxation times can be affected by the spatial distribution of the free radicals which, in turn, depends on the spatial distribution of the energy released by various radiation beams. Therefore, the analysis of the features of ESR signal which depend on the relaxation times can provide information on the radiation quality. Here, three ESR methods are described for discriminating different quality radiations:

- analysis of the continuous wave ESR (cw-ESR) microwave power saturation,
- analysis of the instantaneous diffusion on the decay of Hahn echo by means of pulsed ESR instrumentation and
- analysis of Double Electron-Electron Resonance (DEER) signal through pulsed ESR spectrometers.

In particular, the first method discriminates samples exposed to different radiation beams by studying the different trends of the peak-to-peak amplitude (related to the different homogeneity of the line broadening) of the ESR line, the second method allows to measure the microscopic local concentration of free radicals and the third method furnishes the distribution of the distances among the free radical produced. All methods are reviewed and their application to ammonium tartrate (AT) (an organic compound which has been extensively studied for dosimetric applications [8-13]) samples exposed to ^{60}Co γ-photons, 19.3 MeV protons and thermal neutrons is reported.

For the sake of completeness, a brief description of the energy distribution in matter after the passage of heavy charged particles (such as protons or C ions) and light particles (such as electrons) follows and this will be correlated with what can be detected by ESR techniques.

2. – Defects' distribution in matter

The main effect of the passage of ionizing radiation through matter is the damage of the pre-existing structure and the production of defects. The damage is strictly correlated with the amount of energy transferred to the medium by the projectile, and with the physical and chemical properties of the matter.

As energetic particles penetrate inside organic compounds (such as ammonium tartrate) the radiolysis is the main process which brings about defects, breaks chemical bonds and causes important variations of the molecular structure [14, 15]. In general, energy loss rates and ionization densities depend on the type of particles and on their energy and on the composition and density of the absorbing medium. When electrons enter a medium, they can undergo large-angle deflections in collisions with orbital electrons and can lose a large fraction of their energy in these collisions. Electrons also undergo occasional collisions with nuclei in which they are deflected through large angles and bremsstrahlung photons are emitted. For these reasons, electron tracks are tortuous and their exact shape and length is unpredictable. Furthermore, for a given initial kinetic energy, an electron travels at a much faster speed and experiences less frequent interactions and, therefore, loses its energy more slowly than heavy charged particles such as α particles or C ions. Consequently, the electrons are much less densely ionizing but much more penetrating than heavy charged particles of similar energy. The electrons are considered low LET radiations and give rise to low ionization density. Also γ and X photons are often counted as low LET radiations, even though they are not directly ionizing radiations. In this case usually the *effective LET* is introduced which is the average LET of the secondary electrons produced after the interaction of photons with matter. For low LET radiations the energy is uniformly released inside the entire volume of the medium and a uniform dose distribution is observed. On the other hand, when a heavy charged particle collides with an orbital electron, its direction is virtually unchanged and it loses only a small fraction of its energy because of the ratio of their masses. However, since it encounters a very large number of electrons in medium and it spends more time (with respect to light charged particles) in interacting with them, the total amount of energy released per unit path is larger than for electrons. These particles are therefore classified as high LET radiations and release their energy along the track which is almost straight and therefore the defects are mainly clustered in the neighborhoods of the track. An heavy charged particle passing through a medium causes the formation of the main track by secondary electrons with energies < 100 eV, and δ-tracks by those with energies > 100 eV. Consequently, for high LET particles irradiation the spatial defect distribution comes out to be inhomogeneous, being very high in cylindrical volumes surrounding the

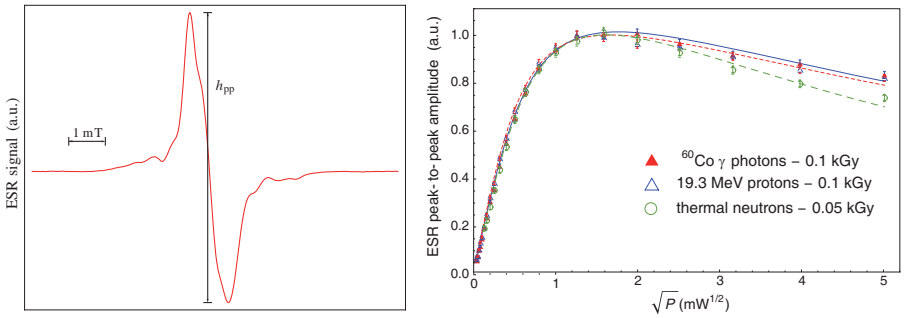

Fig. 1. – Left: ESR spectrum of ammonium tartrate. Right: Trends of the peak-to-peak amplitude *vs.* square root of microwave power for samples exposed to ^{60}Co photons, protons and thermal neutrons. Adapted from [11].

track and very low at great distances from the track if there is no effective migration of the charges and excited states (which are the precursors of the radical products) from the track. Furthermore, if the concentration of free radicals near the track center is very high, recombination and quenching processes can take place and this involves a loss of the total number of defects produced by ionizing radiations.

Therefore, high LET particles will give rise to an energy distribution different from that of low LET particles. It must be underlined that the final spatial distribution of free radicals could differ from the distribution of energy released because the processes of free radicals interaction and/or recombination can modify the radiation yield of radicals' production. The aim of this work is to explain how ESR spectroscopy can provide information on the spatial distribution of free radicals by analyzing the mutual distances among these various paramagnetic centers.

3. – Cw-ESR microwave power saturation method

The first method shown is the analysis of the continuous wave ESR signal with varying the microwave power [11]. This analysis relies on the Castner theory for the inhomogeneously broadened ESR line [16] which is a convolution of a Lorentzian spin packet in a Gaussian envelope:

$$A(B) \propto \frac{B_1}{\Delta B_G \Delta B_L} \int_0^\infty \frac{B' e^{-\left(\frac{B'-B_0}{\Delta B_G}\right)} \mathrm{d}B'}{1 + \left(\frac{B-B'}{\Delta B_L}\right)^2 + \gamma^2 B_1^2 T_1 T_2}, \tag{1}$$

where $A(B)$ is the amplitude of the absorption profile as a function of the magnetic field B; T_1 and T_2 are, respectively, the spin-lattice and spin-spin relaxation times; ΔB_G is the width of the Gaussian distribution of the inhomogeneous broadening; ΔB_L represents the width of a Lorentzian single spin packet and which is inversely proportional to $T_2 (B_L \approx 1/(\gamma T_2))$; B_0 represents the central frequency of the Gaussian distribution; B_1 is the intensity of the microwave oscillating magnetic field; γ is the gyromagnetic ratio for the system under investigation; B' is the running variable.

Experimentally the derivative of the ESR absorption curve is detected; for instance, the ESR spectrum is reported in fig. 1a. The cw-ESR microwave power saturation method aims at studying the dependence of the peak-to-peak amplitude h_{pp} of the main

TABLE I. – *Parameter obtained for the cw-ESR data. These data were reproduced with permission from* [11].

Radiation	LET (keV/μm)	Dose (kGy)	$a/10^{-2}$	$x_0^2 \times T_2$ (mW μs)	T_2 (μs)
1.25 MeV photons	≈ 0.35	0.1	4.0 ± 0.4	1.94 ± 0.11	3.8 ± 0.2
19.3 MeV protons	≈ 4.6	0.1	4.5 ± 0.5	2.00 ± 0.11	3.3 ± 0.2
Thermal neutrons	≈ 70	0.05	5.5 ± 0.6	1.98 ± 0.11	3.0 ± 0.2
1.25 MeV photons	≈ 0.35	1.0	5.3 ± 0.5	2.16 ± 0.11	3.68 ± 0.17
19.3 MeV protons	≈ 4.6	1.0	6.4 ± 0.6	2.06 ± 0.10	2.95 ± 0.13
1.25 MeV photons	≈ 0.35	5.0	7.1 ± 0.6	1.87 ± 0.07	2.64 ± 0.09
19.3 MeV protons	≈ 4.6	5.0	8.8 ± 0.7	1.95 ± 0.08	2.09 ± 0.07

peak of the ESR spectrum as a function of microwave power. In particular, for low mw power P values h_{pp} linearly increases with $\sqrt{P}$, reaches a maximum value and for high values of P decreases. The details of the h_{pp} trends depend on the relaxations times. For the analysis of these trends the expression 1 is suitably approximated [17] and differentiated and used to get the value of the peak-to-peak amplitude for various values of the square root $x(= \sqrt{P} \propto B_1)$ of the mw power. A numerical fitting procedure, which provides as parameters T_2, $a = \frac{\Delta B_L}{\Delta B_g}$ (which gives information about the homogeneity degree of line broadening) and $x_0^2 \times T_2$ (where x_0 is defined by the following expression $(\frac{x}{x_0})^2 = \gamma^2 B_1^2 T_1 T_2$ and therefore the parameter $x_0^2 \times T_2$ is proportional to $1/T_1$), has been developed [11].

Experiments were carried out on dosimeters composed of micro-crystalline power of ammonium tartrate irradiated with three different beams: ^{60}Co γ photons, 19.3 MeV initial energy protons and thermal neutrons at various doses ranging from 0.05 kGy up to 5 kGy (see table I) [11]. For all these beams estimates of LET values were obtained by means of Monte Carlo simulations [13] and are also reported in table I. It should be highlighted that the shape of the ESR spectra of AT samples is apparently independent of radiation quality and dose.

As an example, fig. 1 shows the trends of h_{pp} with varying microwave power for AT dosimeters exposed to ^{60}Co photons (0.1 kGy), 19.3 MeV protons (0.1 kGy) and thermal neutrons (≈ 0.05 kGy).

Table I shows the values of the parameters a, T_2, and $x_0^2 \times T_2$ obtained by numerical fitting procedures on these saturation curves. The values of the parameter T_2, obtained through this microwave power saturation analysis, are just estimates of the real transversal relaxation time.

From table I it can be deduced that the values of the estimates of relaxation time T_2 decrease with increasing LET. This can be explained by considering that for samples exposed to high LET radiation (19.3 MeV protons and thermal neutrons) the free radicals produced are mainly distributed along the track of these particles. Therefore, for these high LET particles a large number of spins are principally concentrated near the core of the track and a small percentage of spin is far away from the path of the ionizing particles. This involves that the dipolar interactions among radicals clustered along the

tracks are more intense and the spin-spin relaxation time is reduced. This finding is confirmed by the values of the a parameter (which is related to the homogeneity of the ESR line and is inversely proportional to T_2); indeed, a reduction of T_2 causes an increase of the a parameter, which, therefore, increases with increasing LET. Furthermore, only small changes are observed for the $x_0^2 \times T_2$ parameter (which is inversely proportional to T_1) and it entails that the longitudinal relaxation time T_1 is less sensitive to the radiation quality and radiation LET.

4. – Measure of the microscopic local concentration

The information obtained by means of the cw-ESR microwave power saturation method above described can provide only estimate of the relaxation properties of the radiation-induced free radicals. In order to get more direct information on the mutual interactions of spins (by measuring the microscopic concentration and the distance distribution of free radicals), pulsed ESR instrumentation is needed. In particular, for the determination of the local spin concentration the two-pulse spin echo sequence (t_1-τ-$2t_1$ where t_1 is the pulse length and τ is the interpulse time) is used [13, 18]. The application of these two pulses gives rises to a spin echo whose intensity depends on microwave power and interpulse time. With increasing τ the spin echo intensity decreases because of random processes related to the spin relaxation. The decay of the echo intensity can be considered exponential with a characteristic time T_m called *phase memory time*. This decay is related to the time fluctuations of the interactions with environment (wherein the electron spin lies) such as the nuclear-electron hyperfine interactions and of the electron-electron interactions. Among the various relaxation processes the *spin diffusion* brings about interactions between different spin packets that exchange magnetization each other causing spin flips. The phase memory time T_m is also affected by the microwave pulses themselves sent to the samples and this phenomenon is called *instantaneous diffusion* (ID). This effect is strongly dependent on the microscopic local concentration of free radicals besides the intensity of the microwave oscillating field.

The measure of the microscopic local concentration involves the application of the 2-pulse electron spin echo (2p-ESE) sequence with varying the interpulse time τ. This provides the echo decay profiles which are analyzed in such a way to disentangle the exponential decay $I_d(\tau)$ (from which the T_m value is extracted) from the modulation contribution $I_m(\tau)$ due to interaction of the electron spins with the nuclear spins. This analysis is carried out for various microwave power values. The dependence of the phase memory time T_m on the microwave power is $\frac{1}{T_m} = A_{SD} + A_{ID}\langle \sin^2 \theta_1 \rangle$ where θ_1 is the tilting angle of the longitudinal magnetization induced by the first pulse, A_{SD} depends on the various intrinsic relaxation processes, including the spin diffusion, and A_{ID}, related to the instantaneous diffusion. In particular, $A_{ID} = \frac{2\pi}{9\sqrt{3}}\gamma^2 h C_A = kC_A$ where γ is the gyromagnetic ratio, h is the Planck constant, and C_A is the microscopic local concentration of the spins affected by the pulses in spins/cm$_3$ [18]; k is then $8.2 \times 10^{-13}\,\mathrm{cm}^3\,\mathrm{s}^{-1}$. From the slope of the linear trends of $\frac{1}{T_m}$ *vs.* $\langle \sin^2 \theta_1 \rangle$ the A_{ID} coefficients are obtained and hence the C_A concentrations are accomplished. The total microscopic local concentration C is obtained by considering the ratio of the number of spin affected by mw pulses to the total number of spins. More details can be found in [13]. In order to highlight the difference between samples exposed to different radiation beams the ratio R of microscopic to macroscopic concentrations is analyzed (see fig. 2). Macroscopic concentration of free radicals can be measured by means of cw-ESR spectrometer by comparing the ESR signal with that of a standard sample of Mn of known spin concentration.

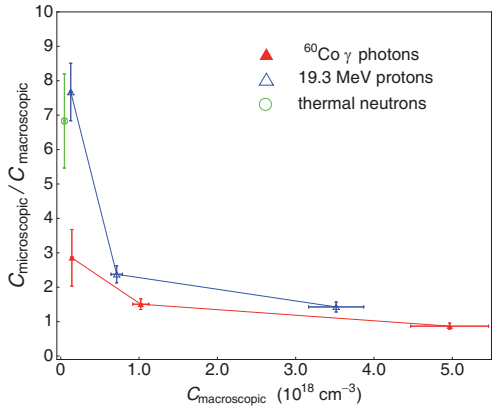

Fig. 2. – Ratio of the microscopic to macroscopic concentration of free radicals as function of macroscopic concentration. Reproduced with permission from [13].

The first evident feature is that R values relative to samples exposed to protons and to thermal neutrons (high LET radiations) is larger than the corresponding value of samples exposed to photons (low LET radiations). This is due to the fact that for high LET radiations the average radical-radical intra-cluster distances are smaller than in case of low LET radiation. In the case of high LET radiations there is near the track axis a high concentration of spins which decreases with distance from the particle path and there are no free radicals far away from the track. In this case a large heterogeneity of the spatial distribution of free radicals is observed. The R values can be much larger than one because the microscopic concentrations are measured in the regions wherein radicals are present (and which in case of low doses are small fractions of the total sample volume) whereas the macroscopic concentrations are obtained as the total number of spins divided by the total sample volume. Furthermore, it should be underlined that the R value for thermal neutrons is a little smaller than for protons even though the average LET ($\approx 70\,\mathrm{keV}\,\mu\mathrm{m}^{-1}$) of the 0.6 MeV protons (released after interaction of thermal neutrons with nitrogen nuclei, *i.e.* $^{14}\mathrm{N(n,p)}^{14}\mathrm{C}$) is one order of magnitude larger than the average LET of the 19.3 MeV protons ($\approx 4.6\,\mathrm{keV}\,\mu\mathrm{m}^{-1}$). This result can be explained considering that phenomena of radical recombination can occur in the case of very high density of energy released (*i.e.* thermal neutron exposure) and the final effect is a reduction of microscopic local concentration of free radicals produced. These recombination phenomena are also responsible for the smaller radical yield observed in case of high LET radiation with respect to photons [19]. On the other hand in the case of γ-photons exposure, the secondary particles (produced after photons'interactions with atoms) are electrons which are able to release energy far away from the interaction site and therefore give rise to a more uniform distribution of free radicals inside the samples. For this reason, the R values are smaller than the corresponding values for the high LET radiations. Moreover, the low amount of energy released per unit path does not favor recombination processes.

Another feature observed in fig. 2 is that the R values tends to one as the absorbed dose increases. This is because for high dose values the spatial distribution of free radicals tends to be uniform (*i.e.* microscopic concentration tends to be equal to macroscopic concentration and $R \to 1$) because the distances among various tracks and radical clusters decrease and the local concentration become almost the same throughout the sample volume. For very high doses the spin interactions are not only among intra-cluster

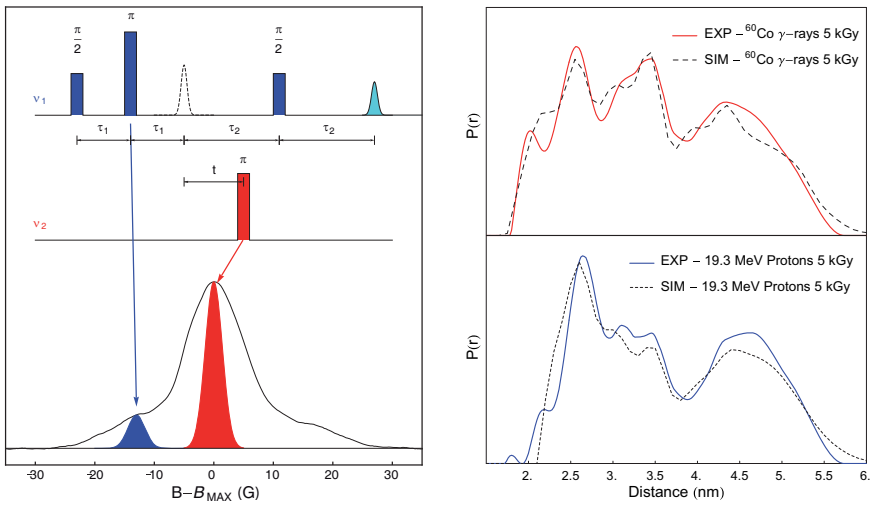

Fig. 3. – Left: Schematic representation of the DEER sequence for ammonium tartrate samples. Right: Distribution of the distance between radicals produced by protons and γ-photons. Reproduced with permission from [13].

radicals but also among radicals belonging to different clusters, since tracks overlap. An estimate of the mean distance of free radicals for high dose values (5 kGy) is about $d = 5.8$ nm. This behavior is found for both proton- and photon-irradiated samples.

5. – Measure of the spin distribution by DEER

The other technique able to discriminate samples exposed to different radiation beams is the the Double Electron-Electron Resonance (DEER). This is an experimental technique which through the analysis of the electron-electron dipolar interaction is able to measure the distance between paramagnetic centers and has found the main applications in the investigation of biological systems [20]. This technique is able to isolate the contribution of the dipolar interaction (which decreases with the third power of the distance between spins) from the exchange interaction (which is negligible for distances larger than 2 nm). The technique is based on the excitation of a group of spin called *pumped B spins* resonating at a frequency ν_2 and on the detection of the changes induced on the signal related to another group of spin called *observed A spins* resonating at a frequency ν_1.

In particular, the sequence is characterized by a 2p-ESE sequence at a frequency ν_1 thanks to which the inhomogeneous broadening of the ESR line of A-spins, also related to various processes such as the g-value dispersion and hyperfine couplings, can be refocused. The application of a π pulse at frequency ν_2 (after the π pulse of the [2p-ESE] at ν_1, see fig. 3, left) causes an inversion of the B-spins. This, in turn, will induce a phase shift $\omega_{ee}t$ on the magnetization of the A-spins where t is the time from the primary echo and $\omega_{ee} = C\frac{1}{r^3}(3\cos(\beta_{AB}) - 1)$ with C is a constant proportional to the product of the g-factors of the two spin groups g_A and g_B, β_{AB} is the angle between the spin-spin vector and the external magnetic field. The acquisition of the final echo amplitude is carried out by varying the time t and the DEER profile is obtained. If the system studied is amorphous, the random distributions of radicals are present and the DEER signal is characterized by simple exponential decays. In case of spin labels

or micro-crystalline systems or in general in systems with distribution of pairs of spins at fixed distances, a signal modulation is detected along with the exponential decay. The analysis of this modulation (which can be performed by means of various softwares such as "DEERAnalysis" [21]) provides the distance distribution of the spins inside the samples. More details on this technique can be found in [20] and reference therein.

Results of the DEER analysis on AT samples exposed to γ photons (5 kGy) and 19.3 MeV protons (5 kGy) are reported in fig. 3, right. The choice of this high dose value is due to the fact that the DEER technique is based on a sequence of three or four pulses and requires a large signal intensity. Regarding the various peaks (centered at 2.0, 2.6, 3.1, 3.4 and 4.5 nm) observed for both kinds of radiations, it should be underlined that only the narrow peaks centered at 2.0, 2.6, 3.1 and 3.4 nm are related to the ionizations produced by a single primary ionization particle (proton or photon) and therefore related to the intra-cluster spin interactions; the broad peak centered at 4.5 nm is strictly correlated to the inter-cluster interactions which are present at this dose value (5 kGy), as stated above.

As can be observed, the two profiles of the distribution of spin distances are different for the two radiation types. The more evident difference is the very intense peak centered at 2.6 nm which has a much more amplitude than other peaks (centered at 2.0, 3.1, 3.4 and 4.5 nm) for proton-irradiated samples. This peak is strictly correlated to the size of the track pattern produced by protons in passing through matter. All peaks in samples exposed to γ-photons have almost equal amplitude and this indicates that a more uniform distribution of free radicals was produced by the secondary electrons generated for this kind of radiation.

Figure 3, right reports also the results of simulation analysis able to describe the distance distribution experimentally observed. In order to computationally simulate the experimental data two factors must be considered: the crystal structure of the ammonium tartrate samples and the spatial distribution of free radicals produced by the ionizing radiations. In particular, for the simulation of photon DEER profile a three-dimensional Gaussian spatial distribution (that is, three 1D Gaussian distribution along three orthogonal axis) was considered, whereas in case of protons the distribution chosen is cylindrical, *i.e.* uniform 1D distribution along the axis of the particle path (neglecting the variations of ionization density as the particle penetrates the sample) and two Gaussian 1D distributions along directions orthogonal to this axis. As can be seen from fig. 3, right, there is a good agreement between experimental data and simulated values.

6. – Conclusions

The contribution of the ESR techniques for the investigation of the spatial distribution of free radicals produced by ionizing radiations is valuable. In particular, the continuous wave-ESR procedure analyzing the peak-to-peak amplitude for various microwave power is able to discriminate radiation with different LETs even though it is not able to provide direct information about the relaxation times of free radicals. The pulsed ESR techniques here described (*i.e.* the *instantaneous diffusion* analysis and the double electron-electron resonance method) are able to provide direct information on the microscopic concentration and distance distribution of free radicals for various ionizing radiation beams. Therefore, these experimental techniques are promising to get a deeper insight on the production of effects of ionizing radiations in organic compounds. More investigations are still needed also on simpler systems such as single crystal samples in order to enhance the knowledge about the formation, migration and/or recombination of

radiation-induced free radicals. If calibration curves for the parameters obtained through these analyses are constructed as function of dose and LET, it could be possible to develop a dosimetric system able to provide information about dose and LET by means of the same dosimeter. Consequently, this kind of dosimeter could find application in radiation therapy optimization because it could furnish information on absorbed dose but also on the quality of radiation. The knowledge of radiation quality is important from a biological point of view and is fundamental for radiation therapy because the biological damage induced by ionizing radiation strongly depends on radiation quality independently of the absorbed dose.

* * *

The author acknowledges funding from the "Neutron dOsimetry and Radiation quality Measurements by Esr and Tl" (NORMET) Project (National Project Leader: Dr. Maurizio Marrale) of the Italian National Institute of Nuclear Physics (INFN) and from the University of Palermo.

REFERENCES

[1] Schardt D., Elsässer T. and Schulz-Ertner D., *Rev. Mod. Phys.*, **82** (2010) 383.
[2] Barth R., *J. Neuro-Oncol.*, **62** (1997) 1.
[3] Spurný F., Jadrníčková I., Bamblevski V. and Molokanov A., *Radiat. Meas.*, **40** (2005) 343.
[4] Gambarini G., Colli V., Gay S., Petrovich C., Pirola L. and Rosi G., *Appl. Radiat. Isot.*, **61** (2004) 759.
[5] Noll M., Böck E., Schöner W., Egger P., Wolf C., Rüdiger H. and Vana N., *Appl. Radiat. Isot.*, **52** (2000) 1135.
[6] Pola A., Moro D., Fazzi A., Colautti P. and Agosteo S., *Radiat. Prot. Dosim.*, **122** (2006) 382.
[7] Regulla D., *Appl. Radiat. Isot.*, **62(2)** (2005) 117.
[8] Brustolon M., Maniero A. L., Jovine S. and Segre U., *Res. Chem. Intermed.*, **22** (1996) 359.
[9] Olsson S., Bagherian S., Lund E., Carlsson G. and Lund A., *Appl. Radiat. Isot.*, **50** (1996) 955.
[10] Brustolon M., Zoleo A. and Lund A., *J. Magn. Res.*, **137** (1999) 389.
[11] Marrale M., Brai M., Triolo A., Bartolotta A. and D'Oca M. C., *Radiat. Res.*, **166** (2006) 802.
[12] Brai M., Gennaro G., Marrale M. and Tranchina L., *Radiat. Meas.*, **42** (2006) 225.
[13] Marrale M., Brai M., Barbon A. and Brustolon M., *Radiat. Res.*, **171** (2009) 349.
[14] Balanzat E. and Bouffard S., *Basic phenomena of tha particle-matter interaction*, in *Materials under irradiation*, edited by Dunlop A., Rullier-Albenque F., Jaouen C., Templier C. and Davenas J. (Trans Tech Publications Ltd) 1993.
[15] J.Davenas, *Ion beam modification of organic materials*, in *Materials under irradiation*, edited by Dunlop A., Rullier-Albenque F., Jaouen C., Templier C. and Davenas J. (Trans Tech Publications Ltd) 1993.
[16] Castner T. J., *Phys. Rev.*, **115** (1959) 1506.
[17] Sagstuen E., Lund A., Itagaki Y. and Maruani J., *J. Phys. Chem. A*, **104** (2000) 6362.
[18] Salikhov K. M. and Tsvetkov Y. D., *Electron spin-echo studies of spin-spin interactions in solids*, in *Time Domain Electron Spin Resonance*, edited by Kevan L. and Schwartz R. N. (Wiley-Interscience, New York) 1979, pp. 231–277.
[19] Lund A., Olsson S., Bonora M., Lund E. and Gustafsson H., *Spectrochim. Acta Part A*, **58** (2002) 1301.
[20] Jeschke G., *Annu. Rev. Phys. Chem.*, **63** (2012) 419.
[21] DEERAnalysis, available at `http://www.epr.ethz.ch/software/index`.